



A novel foam formulation by Al₂O₃/SiO₂ nanoparticles for EOR applications: A mechanistic study

Hosein Rezvani^{a,b}, Donya Panahpoori^a, Masoud Riazi^{a,c,*}, Rafat Parsaei^c, Morteza Tabaei^d, Farid B. Cortés^e

^a Enhanced Oil Recovery (EOR) Research Centre, IOR/EOR Research Institute, Shiraz University, Shiraz, Iran

^b Department of Chemistry and Biochemistry, University of Hull, Hull, UK

^c Department of Petroleum Engineering, School of Chemical and Petroleum Engineering, Shiraz University, Shiraz, Iran

^d Department of Mining Engineering, Isfahan University of Technology, Isfahan, Iran

^e Grupo de Investigación en Fenómenos de Superficie – Michael Polanyi, Facultad de Minas, Universidad Nacional de Colombia Sede Medellín, Cra 80 No. 65-223, 050034 Medellín, Colombia

ARTICLE INFO

Article history:

Received 28 December 2019

Received in revised form 7 February 2020

Accepted 17 February 2020

Available online 19 February 2020

Keywords:

Al₂O₃/SiO₂

Nanoparticles

Foam

CTAB

EOR

bubble-Bubble lamella Division

ABSTRACT

In this study, the influence of Al₂O₃/SiO₂ nanoparticles (NPs) on the Cetyl Trimethyl Ammonium Bromide (CTAB) foam formation and stability is investigated for enhanced oil recovery (EOR). The optimum foaming concentration of CTAB in the presence of heavy crude oil was first determined via visual foam stability inspections for different CTAB concentrations. The results of these sets of experiments were used to find out an appropriate CTAB: Al₂O₃/SiO₂ NPs concentration ratio for foam stabilization through spectroscopy measurements. Different static analyses, including zeta potential, contact angle, and interfacial viscosity measurements were conducted to support the observations in the porous media during flooding. Improved foam stability in the presence of crude oil was observed with Al₂O₃/SiO₂ CTAB foam via electrostatic adsorption of positive CTA⁺ molecules onto the negatively charged NPs at the appropriate concentration ratio of CTAB: NPs. Contact angle measurements showed a similar glass wettability alteration from an oil-wet (155 ± 3°) to a water-wet condition (19–29°) for all blends of CTAB and Al₂O₃, SiO₂, or Al₂O₃/SiO₂ NPs. Foam/heavy crude oil interfacial viscosity measurements increased with the addition of NPs to the foam solutions, indicating an improved foam bubble deformability, viscoelasticity, and stability, which was consistent with the foam behavior in the porous medium. Oil displacement studies in the glass micromodel showed the highest ultimate and incremental oil recovery of 92% and 73% OOIP, respectively, for Al₂O₃/SiO₂ CTAB foam injection in the dual permeability porous medium. Some new forms of conventional foam mechanisms in the porous medium were also observed during the injection of Al₂O₃/SiO₂ CTAB foam, which are believed to be the possible reason for this high ultimate oil recovery. These results prove the efficient role of Al₂O₃/SiO₂ NPs in enhancing the foam performance via synergistic effects of NPs and CTAB.

© 2020 Elsevier B.V. All rights reserved.

1. Introduction

Even though the traditional Improved Oil Recovery (IOR) processes like water and gas flooding hold relatively low operational costs, they face the prospect of several technical challenges, which reduce the process efficiencies. This deficiency comes from lack of a favorable mobility ratio, overriding and underriding by gravity, and fluid fingering [1]. Therefore, they are not favored in dual permeability porous media. To solve these problems, foam flooding has been introduced for EOR and proven to be successful in the laboratory scale [2–5]. There is also a great chance of foam bubble formation during injection of surfactants, alkaline, NPs dispersions, sea/formation water, and steam into the oil reservoirs due to the high salinity/temperature/pressure conditions

and depending on the crude oil/aqueous phase volume. Therefore, the investigation of foam flow and behavior in the porous media is important not only as an EOR method but also as an inevitable in-situ formed phenomenon in the oil reservoirs.

Recently, there has been an interest in foams stabilized by a blend of NPs and surfactants [6–10]. The synergistic advantages of surfactant as a foaming agent and NPs as a stabilizer are boosted in NPs/surfactant foams. Previous studies show that foams stabilized by surfactants and NPs present a high foamability and long-term stability [11,12]. Wettability alteration, interfacial tension (IFT) reduction, prevention of asphaltene deposition, and oil viscosity reduction are also the main improvements that have been reported for NPs in EOR processes [13]. Besides, they can tolerate the harsh environments (i.e. high pressure and temperature conditions) of oil reservoirs, which is not usually true for most surfactants and polymers [14,15].

Over the past years, several studies have addressed NPs-stabilized foam flooding as an EOR method [3,8,16–18]. It is worth mentioning

* Corresponding author at: Enhanced Oil Recovery (EOR) Research Centre, IOR/EOR Research Institute, Shiraz University, Shiraz, Iran.
E-mail address: mrhazi@shirazu.ac.ir (M. Riazi).

that the interaction between surfactants and NPs affect the quality and stability of foams. In this sense, Betancur et al. investigated the influence of the addition of silicon dioxide NPs on the adsorption isotherms of three types of surfactants including CTAB, sodium dodecyl sulfate (SDS) and Tween 20 surfactants before and after micelle formation with a focus on EOR. Their results showed that CTAB has the highest adsorptive capacity and adsorbate-adsorbent affinity. Meanwhile, SDS presents the lowest amount adsorbed on the NPs surfaces [19]. Mo et al. studied the role of various factors affecting the NPs-stabilized CO₂ foam through core flooding experiments at reservoir conditions. They concluded that 0.01 wt% SiO₂ is the optimum concentration and beyond that, the foam mobility declines, ending up with a reduction in foam resistance factor [9]. Aroonsri et al. evaluated the effect of SiO₂ NPs on the foaming efficiency by analyzing apparent viscosity, foam stability, and NPs surface wettability. They also performed some flooding experiments to unfractured and fractured sandstone cores. They concluded that foams are stable at shear rates above a threshold. The value of the threshold shear rate changes with the experimental conditions, including pressure, NPs concentration and wettability, salinity, and temperature. Because high shear rates relate to the oil production from high permeable areas (e.g. fractures), decreasing CO₂ mobility by foam changes the CO₂ movement toward the low permeable areas with unrecovered oil [4]. Manan et al. declared that with the dispersion of Al₂O₃ NPs in the foam aqueous phase, the stability of foam bubbles at the harsh reservoir conditions increases. They studied the effects of different kinds of NPs including SiO₂, Al₂O₃, CuO, and TiO₂ in the presence of Alpha Olefin Sulfonate (AOS) surfactant on the CO₂ foam performance through the foam half-time analysis. They observed that all NPs improved the foam stability at specific concentrations, with Al₂O₃ NPs showing the highest stability [20]. Recently, Bayat et al. investigated the role of the same NPs (SiO₂, Al₂O₃, CuO, and TiO₂) at different concentrations through stability and displacement tests. They observed that highest stability belongs to SiO₂-stabilized foam, which leads to an oil recovery of ~72% original oil in place (OOIP) [21]. According to these results, it is concluded that SiO₂ NPs hold a relative advantage over Al₂O₃ NPs when it comes to the EOR benefits, including wettability, IFT and successful attachment at the oil/water interface. Yekken et al. investigated the effect of silica and ammonia NPs on the SDS adsorption and foam stability. Their results showed that the addition of Al₂O₃ and SiO₂ NPs increases the foam's half-life. They stated that lamella division and bubble-to-multiple bubble lamellae division act as dominant mechanisms of the foam flow. The SiO₂ and Al₂O₃ SDS foams flow multilaterally in the porous media in the presence of oil. They also resulted ~100% OOIP for NPs-stabilized foam flooding, which was attributed to the enhanced film interfacial elasticities [22]. Rognmo et al. questioned the role of two types of hydrophilic silica NPs as a foam stabilizer in the presence of crude oil during supercritical injection of CO₂. They observed improved foam stability and hence increased oil recovery during silica CO₂ foam flooding. The improved foam stability was attributed to the degree of hydrophilicity of two NPs and their different pH. Based on their results, NPs with a lower pH (i.e. pH = 6.5) presented a stronger foam than those at a higher pH (i.e. pH = 8.5) [23]. Risal et al. studied the role of surface-modified silica NPs in the stability and pore plugging of foam bubbles in the porous media. The results of residual oil recovery showed that the NPs-stabilized foam can recover approximately 18% of the residual oil [24]. Kong et al. investigated microscopic blocking characteristics of foam bubbles in a 2D visualization and a 3D core flooding test. After the foam flooding, the incremental oil recovery rates of the high, medium, and low permeability layers were roughly 18%, 20%,

and 23% OOIP, respectively, indicating the influence of heterogeneity and effectiveness of foam flooding [2].

In most previous investigations, the bulk foam stability has been examined only by inspecting the foam height in vertical columns with time or core flooding experiments. However, the dynamic foam stability in the presence of crude oil in the porous medium is of greater importance. Therefore, there is still a paucity of information on the microscopic behavior of NPs/surfactant foams. As mentioned earlier and as available in the literature, Al₂O₃ and SiO₂ NPs have been well proved to be efficient for EOR purposes. In this study, an attempt toward stabilization of CTAB foams by Al₂O₃/SiO₂ NPs for EOR has been made and the resulting foam was compared with the foams stabilized by different NPs including Al₂O₃ and SiO₂ NPs. Therefore, Al₂O₃/SiO₂ NPs were first synthesized and characterized. It was then questioned for improving the efficiency of foam flooding in a heterogeneous dual permeability porous medium through flow visualization studies at optimum concentrations of NPs and CTAB. The effect of the Al₂O₃/SiO₂ NPs on the interfacial viscosity, wettability, and foam stability was also investigated through various static and dynamic studies.

2. Materials and methods

2.1. Materials

A heavy dead crude oil sample was used in this study. The viscosity and density of the crude oil at 25 °C were 160 cP and 0.89 g/cm³, respectively. The SARA analysis performed on the crude oil indicated 41 wt% saturates, 8 wt% asphaltenes, 2 wt% resins, and 49 wt% aromatics.

CTAB (C₁₉H₄₂BrN, >97%, Merck, Germany) and N₂ gas (>99%) were used in this research for foam generation. N₂ gas was chosen in this research because of inertness and its availability due to its ~80% share in the air. γ-Al₂O₃ and SiO₂ NPs were both purchased from the US Research Nanomaterials Inc. (USA) (Table 1). Fig. 1 presents the SEM images of these two NPs provided by the supplier.

Tetraethyl Orthosilicate (TEOS: Si(OC₂H₅)₄, Merck, Germany), Ethanol (C₂H₆O, 99.8%, Merck, Germany), Hydrochloric Acid (HCl, 37%, Merck), and Aluminum Nitrate Nonahydrate (Al(NO₃)₃·9H₂O, 98%, Sigma-Aldrich, USA) were all purchased and used for the synthesis of Al₂O₃/SiO₂ NPs. Deionized water (DIW) was used for the foam preparation.

HCl and Sodium Hydroxide (NaOH, 97%, Sigma-Aldrich, USA) were used for pH adjustment where needed.

2.2. Methods

2.2.1. Synthesis of Al₂O₃/SiO₂ NPs

The sol-gel method was used for synthesizing Al₂O₃/SiO₂ NPs with a ratio of 1:1. The steps were the same as reported by Mobarakeh et al. and Duan et al. [25,26]. TEOS, ethanol, DIW, and HCl were selected with a molar ratio of 1, 22, 13, and 0.00079, respectively. TEOS and ethanol were first mixed and refluxed for 2 h at 75 °C. Aluminum nitrate with the same molar ratio of TEOS: ethanol (1:22) was dissolved in ethanol and stirred for an hour on a magnetic stirrer. Then, the mixture was added to the TEOS and ethanol solution and refluxed at 75 °C for an additional 1 h. Afterward, the solution was cooled at room temperature of 20–23 °C for a day and then dried in two steps: 24 h at 60 °C and 24 h at 80 °C. The dried sample was then calcined at 500 °C with a temperature increasing rate of 8 °C/min for 12 h. X-ray diffraction (XRD) and Transmission Electron Microscopy (TEM) were performed on the final sample.

Table 1
Properties of Al₂O₃ and SiO₂ NPs provided by the US Research Nanomaterials Inc.

Type of NPs	Purity (%)	APS (nm)	SSA (BET m ² /g)	Color	Morphology	Density (g/cm ³)
γ-Al ₂ O ₃	99.0+	20	>138	White	Nearly spherical	3.89
SiO ₂	99.5	20–30	180–600	White	Spherical	2.40

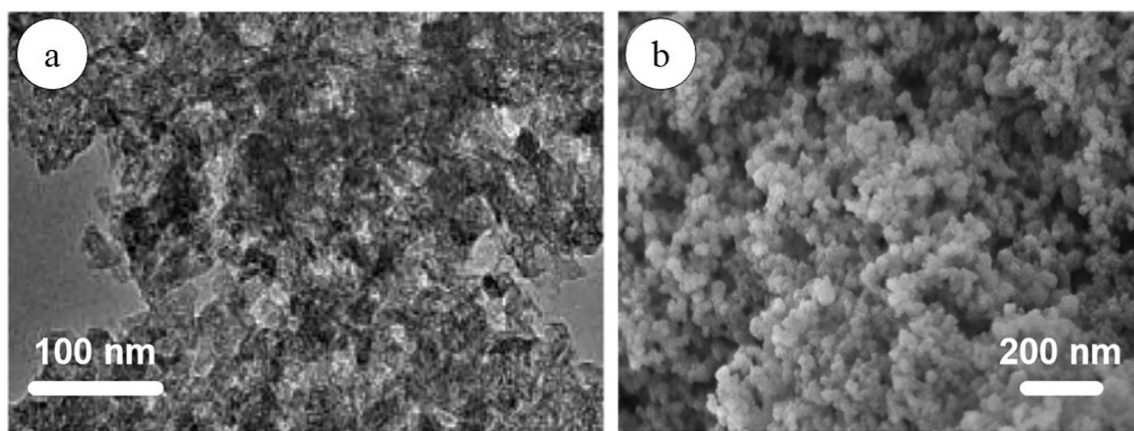


Fig. 1. SEM of (a) Al_2O_3 and (b) SiO_2 NPs.

2.2.2. NPs isoelectric point determination

To determine the isoelectric point and therefore the surface charge of NPs, zeta potential measurements were run for Al_2O_3 , SiO_2 , and $\text{Al}_2\text{O}_3/\text{SiO}_2$ dispersions at 25.0 °C for a pH range of 2 to 10 by Nanopartica SZ-100 (Horiba, Japan). HCl (0.1 M) and NaOH (0.01–0.1 M) were used for pH adjustment.

2.2.3. Determination of optimum CTAB and $\text{Al}_2\text{O}_3/\text{SiO}_2$ NPs concentrations

In this research, the optimum foaming concentration of CTAB was determined in the presence of crude oil through visual foam stability inspections in glass vials. The inspection was performed for different concentrations of CTAB including 0.01, 0.02, 0.03, 0.04, 0.05, 0.06, 0.07, 0.08, 0.09, and 0.1 wt% in DIW. The method included shaking a blend of oil and CTAB solutions with a ratio of 1:4 by volume in a glass vial for 6 s to generate foams. The glass vials were then pictured and the optimum foaming concentration of CTAB was determined by monitoring the foam decay with time.

The Dynamica DB-20S UV/Vis Double Beam Spectrophotometer (Dynamica, Vietnam) was used for the determination of the optimum concentration of $\text{Al}_2\text{O}_3/\text{SiO}_2$ NPs at a fixed concentration of CTAB determined through bottle tests. The measurements were performed at a wavelength of 550 nm and for different concentrations of $\text{Al}_2\text{O}_3/\text{SiO}_2$ NPs (0, 0.02, 0.03, 0.04, 0.05, 0.06, and 0.08 wt%) to find the best CTAB: $\text{Al}_2\text{O}_3/\text{SiO}_2$ NPs concentration ratio for optimum foaming. The wavelength was selected based on the linear part of the overall absorbance spectrum of the $\text{Al}_2\text{O}_3/\text{SiO}_2$ -CTAB dispersion.

2.2.4. Evaluation of wettability alteration

The inverted sessile drop method in DSA100 (Kruss, Germany) was used for evaluating the wettability alteration caused by different dispersions at a constant concentration of NPs and CTAB determined in Section 2.2.3. The measurements were performed on glass surfaces at the room pressure and temperature of 1.00–1.02 bar and 20–26 °C, respectively. Glass surfaces were used to facilitate the comparison of wettability alteration at the static and dynamic states. To reach a completely oil-wet condition, glass surfaces were treated in stearic acid dissolved in *n*-heptane (typically 0.018 M) for 48 h. The contact angle measurement method can be found elsewhere [27–29]. Briefly, it includes the injection of the same droplet volume of crude oil (6 μL) on the glass surface and measuring left/right contact angles. The values were then averaged, and error bars are given.

2.2.5. Evaluation of foam/crude oil interfacial viscosity

The MCR-302 Rheometer (Anton Paar, Austria) was used for measuring the interfacial viscosity between the $\text{Al}_2\text{O}_3/\text{SiO}_2$ CTAB foam and crude oil at the room conditions.

2.2.6. Glass micromodel study

An etched glass micromodel was used to investigate microscopic and macroscopic oil displacement during injection scenarios (Fig. 2). The experimental setup included an N_2 gas cylinder, a mass flow controller (MFC) for gas flow regulation, a syringe pump for injection of fluids, a microscopic camera (Dino-lite Digital Microscope, Taiwan) for monitoring the fluid displacement, the glass micromodel (i.e. porous medium), a white light source, a PC, and a differential pressure (DP) gauge to record pressure differences during injection scenarios. In this research, foams were formed via co-injection of N_2 gas and NPs/CTAB dispersions prior to the injection into the porous medium.

The porous medium was 7.0 cm in length and was made by etching a look-alike sandstone rock pattern on a glass surface using a laser beam. The porosity and average depth of the pores were 40% and ~60 μm , respectively. The porous medium consisted of two permeability zones: one with broad and the other with narrow pore throat sizes. The average width of pore throats in the high and low permeable regions was 180–200 and 100–120 μm , respectively.

Table 2 indicates different secondary and tertiary injection scenarios run for the oil displacement study. In each experiment, the porous medium was first evacuated, saturated with crude oil, and then aged for a day to become completely oil wet. The secondary injection mode included 1 pore volume (PV) injection of DIW into the micromodel. The tertiary injection mode included 1 PV injection of DIW, N_2 gas or different foams into the micromodel. All experiments were performed at the ambient pressure (1.00–1.02 bar) and ambient temperature (18–23 °C) with no effect of gravity as the micromodel was placed horizontally. During each experiment, the microscopic and macroscopic imaging technique was conducted continuously to monitor the foam behavior and oil displacement by different injected fluids. The oil recoveries and pressure differences were also recorded.

3. Results and discussions

3.1. Characterization of $\text{Al}_2\text{O}_3/\text{SiO}_2$ NPs

The properties of a material like crystal structure is highly related to the atoms and the way they are arranged in its structure, which can be easily determined through XRD patterns. There are two different kinds of materials. Those materials with atoms randomly arranged like liquids and without any ordered network, which are called “Amorphous Materials”. The second group includes materials with atoms in an ordered arrangement in which the pattern is spatially repeated in three directions, which are called “Crystalline Materials”. Silica belongs to the first categorization and when it is used on the surface of other NPs as a coating agent, it affects its XRD pattern and reduces the intensity of the sharp

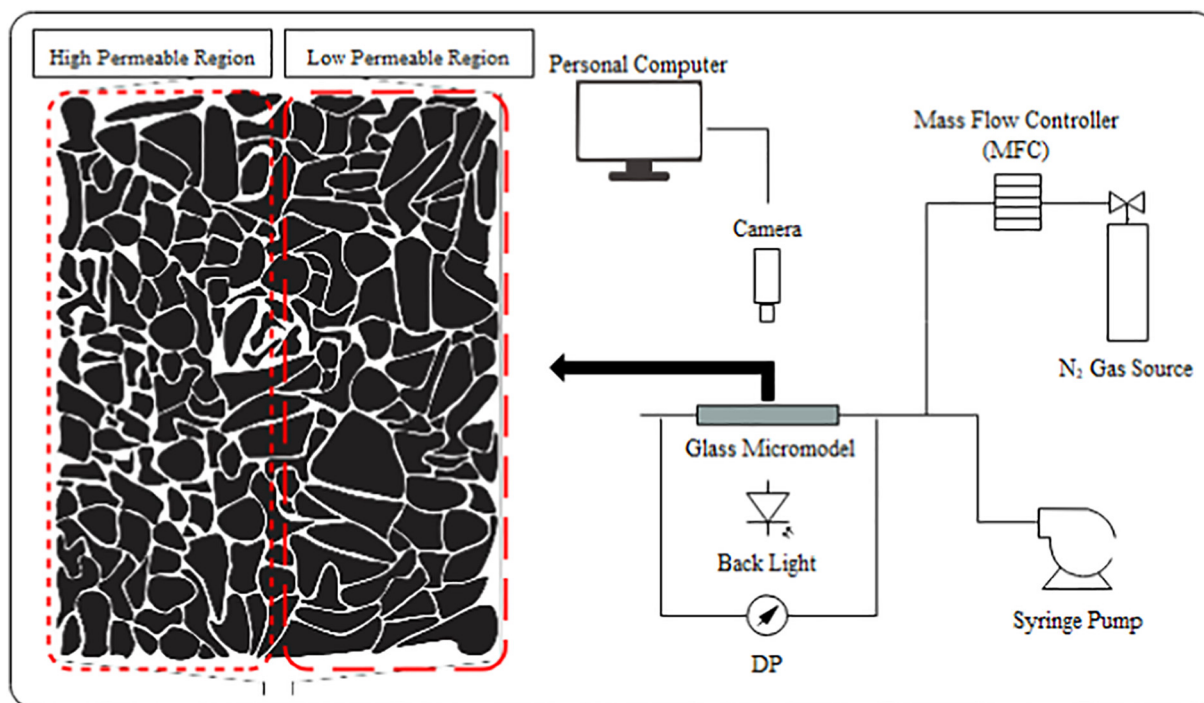


Fig. 2. Set-up used for foam flooding.

peaks, which is indicative of altering the structure [30]. The XRD patterns of Al_2O_3 NPs and the $\text{Al}_2\text{O}_3/\text{SiO}_2$ NPs are shown in Fig. 3. The index peaks have been determined on the XRD pattern of $\text{Al}_2\text{O}_3/\text{SiO}_2$ NPs in Fig. 3b. The pattern confirms the successful coating of silica on Alumina during synthesis. As it is shown, the index peaks of Al_2O_3 NPs have been reduced by coating with silica. This would convert the ordered skeleton of Al_2O_3 NPs to an amorphous structure (Fig. 3b).

Fig. 4 illustrates the TEM image of the $\text{Al}_2\text{O}_3/\text{SiO}_2$ NPs. The figure shows a nearly spherical morphology and confirms the successful coating of silica on alumina with a final average size of 50 nm.

3.2. Stability of Al_2O_3 , SiO_2 , and $\text{Al}_2\text{O}_3/\text{SiO}_2$ NPs in aqueous phase

The zeta potential measurements of 0.04 wt% Al_2O_3 , SiO_2 , and $\text{Al}_2\text{O}_3/\text{SiO}_2$ NPs in DIW at different pH of 2 to 10 are shown in Fig. 5. For each dispersion, three zeta potential measurements were carried out and the average/error bar was calculated. The figure shows that zero-point charge (ZPC) of Al_2O_3 , SiO_2 , and $\text{Al}_2\text{O}_3/\text{SiO}_2$ are at pH 6.7, 2.7, and 5.1 at 25 °C, respectively. On the other hand, the pH of blends of CTAB and Al_2O_3 , SiO_2 , or $\text{Al}_2\text{O}_3/\text{SiO}_2$ NPs used for flooding in this study were 8–9, 6–7, and 7–8 at 25 °C, respectively, which are all above their corresponding ZPC values.

Table 2

Various injection scenarios for investigating the oil displacement in the glass micromodel.

Flooding no.	Secondary injection (1 PV)	Tertiary injection (1 PV)
1		DIW
2		N_2 gas
3		CTAB foam
4	DIW	Al_2O_3 CTAB foam
5		SiO_2 CTAB foam
6		$\text{Al}_2\text{O}_3/\text{SiO}_2$ CTAB foam

Alzobaidi et al. proposed a new parameter called “hydrophilic/ CO_2 -philic balance”, similar to the hydrophilic-lipophilic balance of surfactants, for foam stabilization by NPs and declared that highly hydrophilic

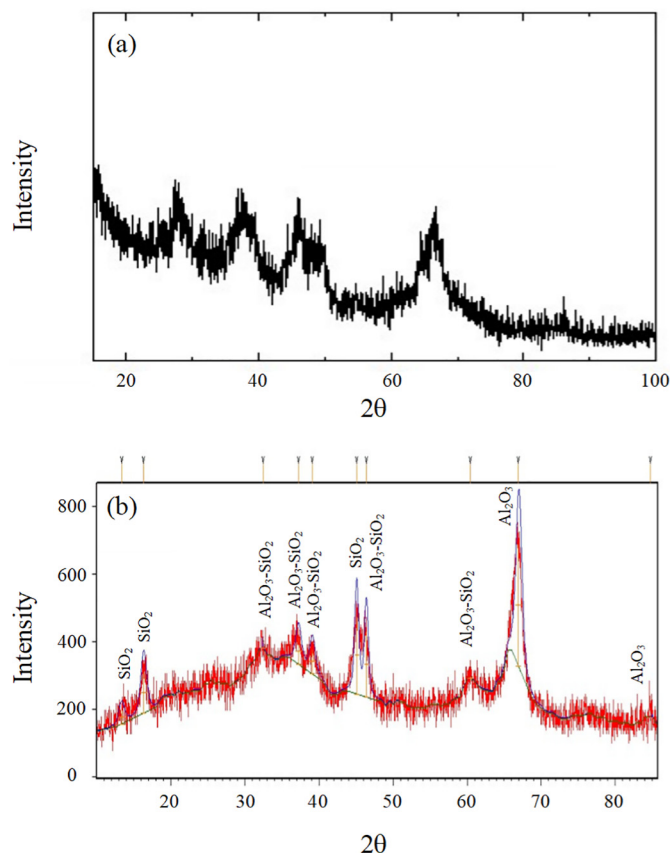


Fig. 3. XRD pattern of (a) Al_2O_3 and (b) $\text{Al}_2\text{O}_3/\text{SiO}_2$.

NPs are not suitable for foam stabilization as they cannot move toward the gas/water surface and tend to stay in the aqueous phase [11]. On the other hand, highly hydrophobic particles (particle/water contact angles above 90°) act like antifoaming agents by a phenomenon called “bridging-dewetting” [31]. Therefore, it is concluded that for foam stabilization, the particles should have a partial hydrophilicity/hydrophobicity. Since in this study, the pH of dispersions was above pH_{ZPC} and silanol (SiOH) groups are available on the surface of the silica, the surface of SiO_2 and $\text{Al}_2\text{O}_3/\text{SiO}_2$ NPs is hydrophilic and negatively charged. In addition, positively charged CTAB was chosen to render the hydrophilicity of the surface by electrostatic adsorption onto the NPs surfaces and thus reducing the contact angle of particles at the N_2 /water surface. According to the ZPC and pH values, for SiO_2 and $\text{Al}_2\text{O}_3/\text{SiO}_2$ NPs, the surface charge density is high as the pH is well above the ZPC values. Therefore, in the blends of CTA^+ with SiO_2 or $\text{Al}_2\text{O}_3/\text{SiO}_2$, there is a strong electrostatic attraction between the positively charged head group of CTA^+ (i.e. quaternary ammonium) and negatively (because of dissociation of silanol groups) charged SiO_2 or $\text{Al}_2\text{O}_3/\text{SiO}_2$ NPs, which modifies the NPs surfaces. CTA^+ tends to adsorb onto the particle surface with the positive head charge oriented toward the particle surface and the alkyl chain toward the solution. This interaction modifies the surface of the particles and makes them less hydrophilic, thus suitable for the surface attachment [19,31–33]. There is a similar interaction between CTA^+ and negatively charged alumina [34].

3.3. Determination of optimum foaming conditions

The CMC of CTAB in the water at 25°C is ~ 0.03 wt%, which has been considered as the optimum foaming concentration when no NPs and crude oil is available in many studies [32,35,36]. At the N_2 /water surface in the absence of crude oil, the CTA^+ monomers are oriented with the alkyl chain toward the N_2 gas in the bubble and the head group toward the water. Many researchers have also studied the effect of CTAB concentration on the foam stabilization without crude oil [31,37,38]. Generally, the results show that the foam volume does not increase above the CMC of CTAB at ~ 0.9 mM (~ 0.03 wt%), beyond which the air/water surface is saturated with the surfactant molecules and there is no significant reduction in the air/water surface tension due to the formation of hydrophilic micelles which tend to stay in the aqueous phase rather than moving toward the air/water surface [32].

In the presence of crude oil, the optimum surfactant concentration is usually above the CMC owing to the possible negative role of crude oil in

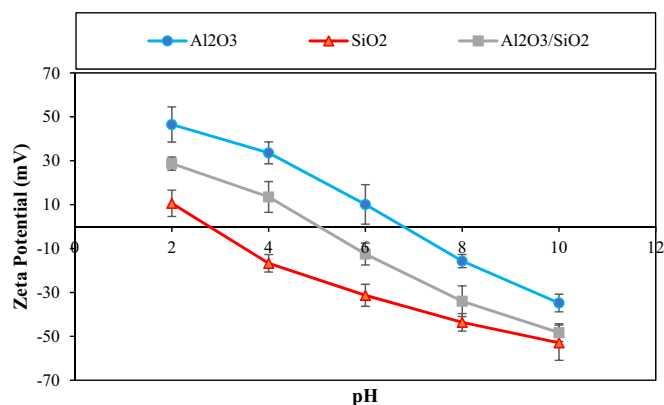


Fig. 5. Zeta potential measurements for different dispersions.

the system. Farajzadeh et al. reviewed the main negative mechanisms of crude oil as an anti-foaming agent when in contact with foam [39]. Fig. 6 shows the results of visual foam stability inspections for the determination of the optimum foaming concentration of CTAB in the presence of a crude oil sample (without NPs). The figure indicates that the optimum foaming concentration of CTAB in the presence of the crude oil sample is 0.08 wt%, which is >2.5 times as large as its CMC. When crude oil is added, the positive head groups of CTA^+ monomers at the N_2 /water surface interact strongly with the negatively-charged components of crude oil such as carboxylic acids and aldehydes, which may lead to the ion-pair formation [38]. Besides, there might be a decrease in the CTAB concentration as surfactant loss at the N_2 /water surface due to the transfer of some CTA^+ monomers into the oil/water interface or the oleic phase of the crude oil. Therefore, it is obvious that the optimum CTAB concentration in the presence of crude oil goes beyond the CMC, depending on the extent of interactions between CTA^+ monomers and oil components.

The figure also indicates that with an increase in CTAB concentration from 0.02 to 0.08 wt%, foaming and foamability increase considerably. Beyond 0.08 wt%, a decrease in the foam height in the glass tube is observed due to the chain-to-chain interaction of CTA^+ monomers, which creates hydrophilic aggregates, tending to stay in the aqueous phase. This could be detrimental to foam stability by lamella rupturing. Thus, the most stable foam in the presence of crude oil is observed with 0.08 wt% CTAB.

The contact angle of silica particles with pure water has been found to be at $\sim 38^\circ$ [37], which indicates a hydrophilic surface wettability for silica and is not suitable for foam stabilization as they cannot attach at the N_2 /water surface efficiently. Generally, contact angles close to the neutral state (90°) are of interest for foam stabilization, which can be performed by surface charge modification [37]. Bi et al. resulted that with the monolayer adsorption of CTA^+ molecules onto the silica surface, the maximum water/particle contact angle would be 84° [33]. Many authors observed that there is a specific CTAB to particle concentration ratio at which the highest foam stability (without crude oil) is observed [31,37]. In this research, regarding the fixed concentration of CTAB (i.e. 0.08 wt%) determined as the optimum foaming concentration in the presence of crude oil in the previous step, an attempt toward the determination of appropriate $\text{Al}_2\text{O}_3/\text{SiO}_2$ concentration was made via spectroscopy analysis. Fig. 7 shows the results of absorbance measurements of $\text{Al}_2\text{O}_3/\text{SiO}_2$ -CTAB dispersions for different concentrations of $\text{Al}_2\text{O}_3/\text{SiO}_2$ at a constant 0.08 wt% CTAB concentration at the wavelength of 550 nm. The cross point of two trend lines in this figure indicates the optimum $\text{Al}_2\text{O}_3/\text{SiO}_2$ concentration in which the highest foamability of $\text{Al}_2\text{O}_3/\text{SiO}_2$ -CTAB solutions is observed in the presence of crude oil. At low NPs concentration below 0.04 wt%, the number of CTA^+ monomers in the solution is high, as compared to the particle number. Therefore, initially, there is a monolayer of the CTA^+ monomers by electrostatic

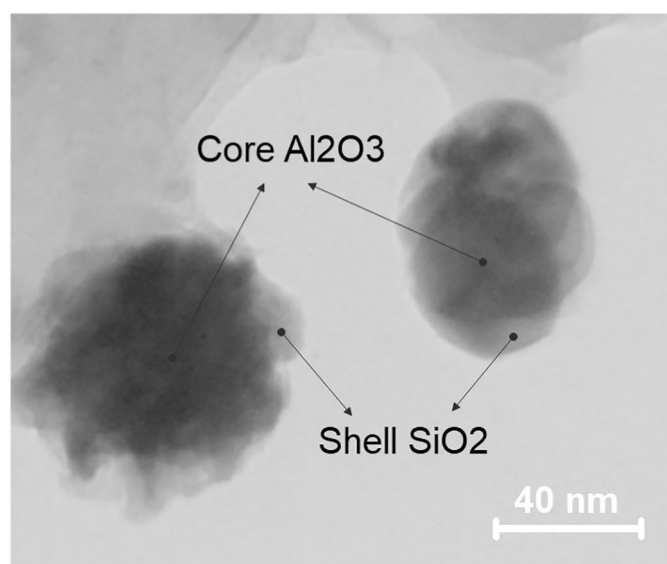


Fig. 4. TEM of the synthesized $\text{Al}_2\text{O}_3/\text{SiO}_2$ NPs.

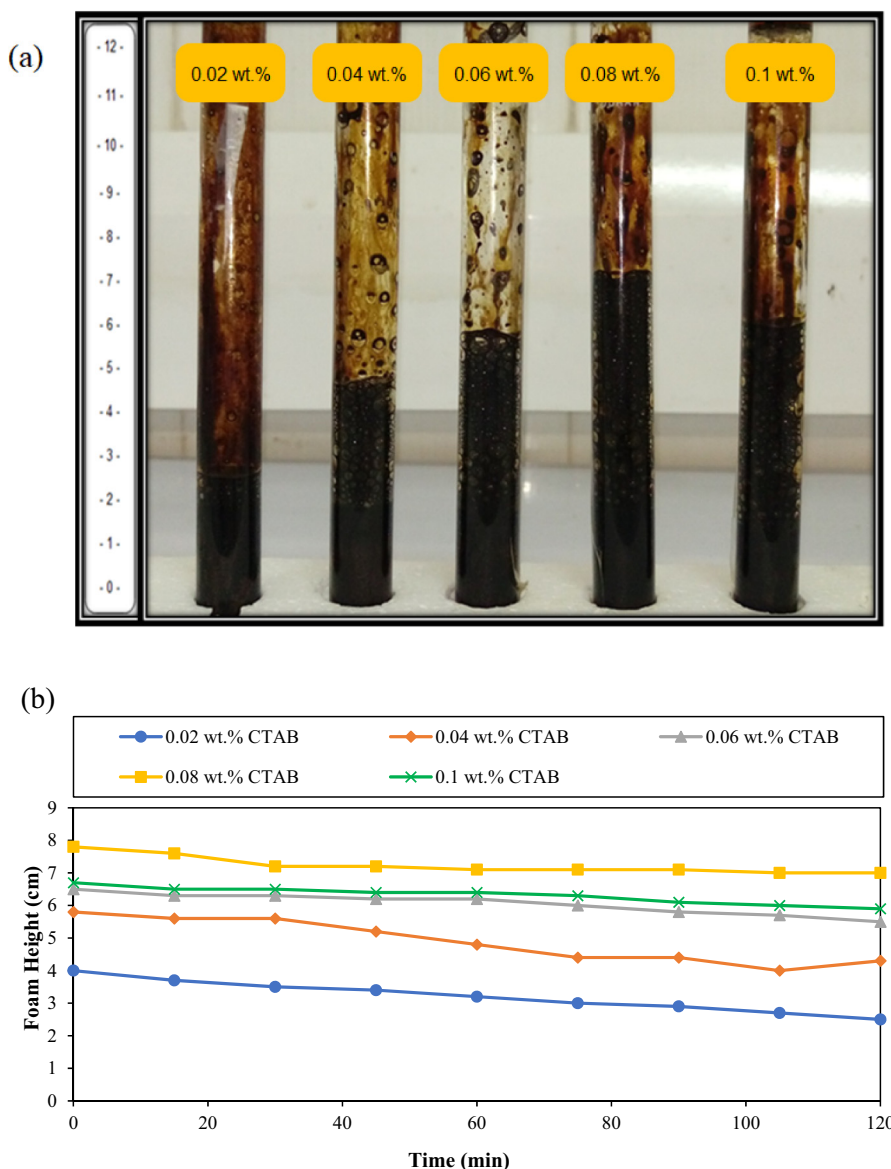


Fig. 6. (a) CTAB Foam stability in the presence of crude oil in glass bottles after 120 min. (b) Foam decay for different concentrations of CTAB surfactant (Oil: foam solution ratio was 1:4 by volume).

adsorption of CTA^+ molecules onto the particle surface. Later, there is a great chance of chain-to-chain interactions via van der Waals forces

between CTA^+ monomers attached to the particle surface and those at the bulk. This phenomenon is similar to the hemi-micelle phenomenon in the bulk and makes the particles highly hydrophilic and unsuitable for attachment at the N_2/water surface as they tend to stay in the aqueous phase [31,32]. At 0.04 wt%, an appropriate ratio of NPs to CTAB concentration ratio is reached and the highest stability was observed. Above 0.04 wt%, the number of CTA^+ monomers in the system relative to the particle number is not sufficient for complete modification of $\text{Al}_2\text{O}_3/\text{SiO}_2$ NPs to be more hydrophobically efficient for foam stabilization. Therefore, 0.04 wt% $\text{Al}_2\text{O}_3/\text{SiO}_2$ and 0.08 wt% CTAB were kept constant as the optimum foaming concentrations of NPs and surfactant in all the following experiments.

3.4. Wettability evaluation

Table 3 summarizes different contact angles of oil droplets on the glass surface in the presence of various surrounding fluids. The pictures and values in this table were taken after the injection of a crude oil droplet on the surface. As indicated in Table 3, the contact angles for blends of NPs and CTAB are significantly small, which show intense hydrophilicity

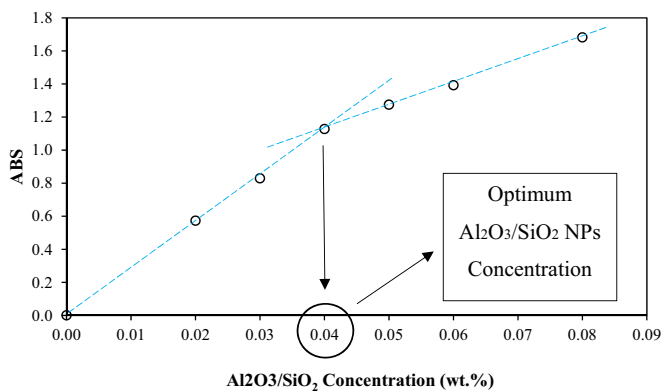


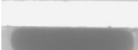




Fig. 7. Absorbance measurements of different concentrations of $\text{Al}_2\text{O}_3/\text{SiO}_2$ NPs at the constant concentration of CTAB (0.08 wt%) and the wavelength of 550 nm.

Table 3
Contact angle measurements of crude oil droplets on the glass surface with different surrounding fluids.

Type of surrounding fluid	Contact angle (degree)	Drop shape
DIW	157 ± 3	
0.08 wt% CTAB	37 ± 2	
0.04 wt% Al ₂ O ₃ + 0.08 wt% CTAB	29 ± 1	
0.04 wt% SiO ₂ + 0.08 wt% CTAB	24 ± 2	
0.04 wt% Al ₂ O ₃ /SiO ₂ + 0.08 wt% CTAB	19 ± 2	

of glass surfaces after treatment. Therefore, it was not possible to monitor the dynamic contact angle for these dispersions as it was impossible to make the oil droplet fixed on the glass surfaces due to the high hydrophilicity. The table shows that the contact angle of the oil/DIW/glass surface is 157°, which is indicative of an initial strongly oil-wet condition. It also indicates that silica NPs bring a higher wettability alteration, as compared to the alumina. That is why one can observe that the synthesized Al₂O₃/SiO₂ NPs presented the lowest contact angle of 19°.

Regarding the effect of CTAB on the rock wettability, it is worthwhile noting that the interaction of CTA⁺ molecules with polar components of crude oil (i.e. hydroxyl groups) on the rock surface plays an important role in the intensification of water-wetness of the rock surface. There are several mechanisms of wettability alteration for micellar solutions like CTAB. The first one is the roll-up in which the contact angle is receding and therefore the oil droplet is removed from the surface. The other mechanism is diffusion that creates a second contact line. Another proposed mechanism is the emulsification in which an attached oil droplet is released due to the decrease in oil/water IFT, leading to the oil in water emulsification. However, there are two main problems with using surfactants alone for EOR: high adsorption onto the rock surface around the injection well and their possible desorption from the rock surface [40]. This has led to the introduction of NPs into this area.

The dominant mechanism for wettability alteration induced is the self-layering of surface-modified NPs on the surface, which is performed through the adsorption of NPs [41]. With the addition of surface-modified NPs to the base fluid, the three-phase contact line quickly reduces for reaching an equilibrium. In this situation, surface-modified NPs begin to arrange in the space between oil and solid surface, namely the wedge region, which applies disjoining pressure on the surface of the glass. The intensity of disjoining pressure decreases with a distance from the wedge layer and is a function of NPs concentration, stability, size, and charge [41]. Therefore, a transition region is formed between the oil droplet on the glass surface and the bulk meniscus. The shape of this profile is highly dependent on the forces applied by ordered NPs or CTAB molecules [42]. Adsorption of surface-modified NPs intensifies the disjoining pressure. This results in the detachment of oil droplets from the surface. In fact, an increase in spreading and frictional coefficients in the contact region improves the oil detachment [41]. Irreversible adsorption of NPs onto the rock surface is the other possible mechanism by which the surface alters to the water-wet state [43–45], which is not true for surfactants alone.

3.5. Foam/crude oil interfacial viscosity

Interfacial rheology becomes significant when two mobile immiscible phases contact each other. In fact, it copes with the interfacial flow

and is pivotal when it comes to the evaluation of the interfacial stress and the shape of the flowing phases. In colloidal systems, such as foams and emulsions, there is a large interfacial area, which makes them thermodynamically unstable [46]. This is particularly a matter of much more importance in the presence of surfactants (i.e., natural surfactants of the crude oil and those added to the water phase) since they can move to the interface and apply further stresses other than ordinary stresses applied by IFT, which ultimately affects the interfacial rheology. In this regard, any alteration in surfactant concentration or temperature of the system alters the surface tension and in turn, brings instability in the system. This is called “Marangoni effect” and leads to convection in the bulk phases caused by the ensuing surface tension gradient in the system [47].

Interfacial features not only have a big influence on foams and emulsions but also affect the process of foaming and emulsification. One of the most important rheological parameters in surfactant-containing systems is the surface shear viscosity; however, it is insignificant in surfactant-free systems [48].

Foam can be regarded as a three-dimensional structure of various lamellae, which are under the influence of drainage and flow. With any disturbance at the interface, the adsorption equilibrium is disturbed and therefore surfactants move toward the interface through Marangoni flow or the coupled bulk phase to bring the equilibrium back. As a result, the surface tension changes. In this regard, foaming and foam stability is a function of compression elasticity and viscosity. Surface viscosity can show the ability of the system for forming stable lamella. Basically, when a surfactant is present in the aqueous phase, they tend to move toward gas/water surface because of their amphiphilic structures. At gas/water surface, the hydrophilic head of surfactant molecules is toward aqueous phase and the tails are oriented toward the gas. Initially, at low surfactant concentrations below CMC, a single layer of distant surfactant molecules is formed at the surface. Increasing surfactant concentration up to CMC makes their packing more compact [49]. With the monolayer adsorption of surfactants, the surface becomes viscoelastic and deformable as the surface tension reduces significantly [46,47]. A viscous surface can restrain the distortions and prevent the bubble ruptures. In this regard, the presence of NPs in the foam solution can improve the dilational viscoelasticity and prevent lamella rupturing by delaying the drainage and acting as a steric barrier [46,47,50].

Fig. 8 shows the interfacial viscosity between 0.08 wt% CTAB foam and crude oil at different shear rates for 0.04 wt% of different NPs in the foam aqueous phase. In all cases, interfacial viscosity decreases almost linearly with an increase in the shear rate. The lowest interfacial viscosity at different shear rates is observed for CTAB foam, while the highest one belongs to the CTAB foam containing Al₂O₃/SiO₂ NPs. It is

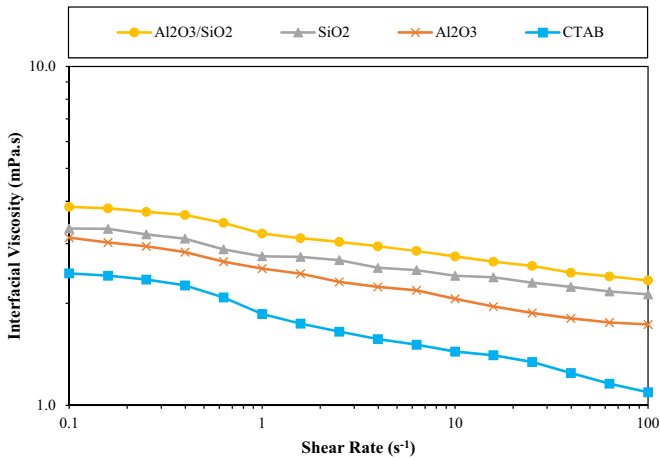


Fig. 8. Interfacial viscosity of 0.08 wt% CTAB foam/crude oil in the presence and absence of 0.04 wt% Al_2O_3 , SiO_2 , and $\text{Al}_2\text{O}_3/\text{SiO}_2$ NPs.

also clear that, in comparison with SiO_2 NPs, there is a further decrease in the interfacial viscosity when Al_2O_3 NPs are added to the foam solution. Therefore, it is not far surprising that SiO_2 -coated Al_2O_3 NPs hold the highest interfacial viscosity values.

Assuming a plane of foam bubbles in contact with crude oil, the interfacial area concentration (β) can be explained as follows [51]:

$$\beta = \frac{A}{V} \quad (1)$$

where A is the total bubble surface area and V refers to the total bubble volume. This parameter is useful in defining the surface tension of each bubble. When there is a compact and dense arrangement of bubbles (small and stable bubbles), the interfacial area concentration is high and therefore a high shear resistance to lamella rupturing exists. Considering the void fraction (α) as follows [51]:

$$\alpha = \frac{n \times \pi d^3}{6V} \quad (2)$$

The interfacial area concentration can be stated as follows:

$$\beta = \frac{A}{V} = \frac{n \times \pi d^2}{2V} = \frac{3\alpha}{d} \quad (3)$$

According to Eq. (3), interfacial area concentration has a direct relationship with a void fraction (α) and is inversely proportional to the foam bubble diameter (d). This implies that small bubbles (stable bubbles) have high interfacial area concentration and in turn have stronger interfacial viscosity. Now, based on the results shown in Fig. 8, $\text{Al}_2\text{O}_3/\text{SiO}_2$ NPs presented the highest interfacial viscosity, indicating that it has caused the most stable bubble foams in contact with crude oil. This result is consistent with other previous observations and the results of oil displacement in the glass micromodel (see Section 3.6).

Generally, the addition of NPs to the foam solution does not reduce the IFT between crude oil and foam as low as CTAB foam; however, it introduces a more viscoelastic interface. This rigidity at the interface indeed prevents lamellae from rupturing and consequently keeps the foam bubbles more stable [50].

3.6. Oil displacement study

In the following sections, the microscopic and macroscopic results, as well as the oil recoveries and pressure differences during the injection of different fluids are discussed.

3.6.1. Macroscopic view of oil displacement

Fig. 9 shows the fluid distribution of the micromodel after the injection of various fluids. Overall, comparing the efficiency of the tertiary methods (Fig. 9c to g), one can notice that the $\text{Al}_2\text{O}_3/\text{SiO}_2$ CTAB foam had the best performance since it has displaced a large amount of original oil after both 0.5 PV (i.e. less injected volume, more economical) and 1 PV (i.e. high sweep efficiency).

As it is shown in Fig. 9b, a quick breakthrough of the DIW through the high permeable zone was observed after ~ 0.3 PV as a secondary injection mode, which led to a low sweep efficiency. This is mainly due to the high oil/water IFT and oil-wet wettability of the medium and confirms the inefficiency of water flooding in oil-wet dual permeable porous media for increasing oil production and the necessity of an improved EOR method. It is also worth noting that DIW injection was continued for 1 PV, however, no considerable further oil recovery was observed.

Another substantial feature in Fig. 9 is that tertiary N_2 gas injection is not effective in sweeping the oil in the porous medium as it basically moves through the DIW-swept areas (Fig. 9c). Due to the unfavored mobility ratio (i.e. low viscosity and high relative permeability), the gas cannot displace the oil toward the production [1].

With the injection of CTAB foam (Fig. 9d), the amount of swept oil after 0.5 PV is not noticeable; nevertheless, this is relatively acceptable after 1 PV as compared to DIW flooding however it seems to be more room for further oil production. The thickness of the oil films, in this case, is thinner owing to the oil/water IFT reduction, which causes the capillary force to decrease and more oil to be produced.

It is interesting to mention that $\text{Al}_2\text{O}_3/\text{SiO}_2$ CTAB foam has displaced almost all the original oil in the porous medium after 1 PV, the amount which was not observed with Al_2O_3 and SiO_2 CTAB foams (Fig. 9: e, f, g). In addition, comparing 0.5 PV pictures related to different injected fluids, it is obvious to note that $\text{Al}_2\text{O}_3/\text{SiO}_2$ CTAB foam has the largest oil sweep efficiency (i.e. less injected volume, more economical). This emphasizes the effective role of $\text{Al}_2\text{O}_3/\text{SiO}_2$ NPs in improving the foam performance for oil displacement. In Section 3.6.2, the main mechanisms for the higher relative efficiency of $\text{Al}_2\text{O}_3/\text{SiO}_2$ CTAB foam have been presented and where necessary, the static results were incorporated to support the observations.

3.6.2. Microscopic mechanisms

- Wettability Alteration

Fig. 10 shows the wettability alteration of pore throats induced by different injected fluids into the porous medium. On account of the long contact time between the glass surface and crude oil during the aging process, the wettability of the glass surfaces turned oil-wet. As a result, residual oil is mainly observed in the form of continuous films over almost all grain surfaces throughout the flooding area.

As indicated in the figure, DIW and N_2 gas cannot remove the oil layers from the grain surfaces because of weak interactions between injected fluid and the heavy crude oil layers on the grains (Fig. 10: a, b). On the other hand, with the addition of NPs, the oil films on the grain surfaces have been decreased. This wettability alteration results from the synergistic effects of NPs and CTAB in the system, as discussed in Section 3.4.

- Pore Plugging Mechanism by Gas Bubbles

NPs aggregation is potentially a problem for foam flow, especially in tight porous media since it enhances the plugging of smaller pore throats, which decreases the foam sweep efficiency [52]. This phenomenon completely differs from the foam blockage mechanism, which is defined as the foam's ability to block larger flow pathways and divert the flow toward smaller zones for more oil production [6]. The microscopic images in



Picture Name	Injected Fluid	Injection Mode
a	oil-saturated porous medium	-
b	DIW	secondary
c	N ₂ Gas	
d	CTAB foam	
e	SiO ₂ CTAB foam	tertiary
f	Al ₂ O ₃ CTAB foam	
g	Al ₂ O ₃ /SiO ₂ CTAB foam	

Fig. 9. Macroscopic view of the porous medium after injection of different fluids. In all cases, the CTAB and NPs concentrations are 0.08 wt% and 0.04 wt%, respectively.

Fig. 11 disclosed that the gas bubbles can plug the pores during Al₂O₃/SiO₂ CTAB foam injection, which can subsequently increase the sweep efficiency by diverting flow into unswept areas and increasing oil recovery. The figure also illustrates a typical example of the foam blockage mechanism during the injection of Al₂O₃/SiO₂ CTAB foam into the porous medium. As shown in Fig. 11a, owing to the foam blockage in pathways number 1 and 2, foam diverts the flow to pathway number 3, which displaces the unrecovered oil in this channel.

Fig. 11b shows the foam transporting and blocking (Gas bubble bridge plugging) mechanism during the tertiary injection of Al₂O₃/SiO₂ foam into the porous medium. Flow blockage by foam bubble number 2 happens in the porous medium (Fig. 11b₂) with the passage of time, leading to the flow diversion of foam bubble number 1 toward the other areas in porous media (Fig. 11b₃). Therefore, it is worth mentioning that foam flooding comes with a good profile control ability in heterogeneous formations and can improve sweep efficiency by blocking large pore throats and diverting the fluid to the areas with lower permeability.

- Gas Bubble Deformations in Porous Medium

Fig. 12 illustrates the gas bubble deformation in the porous medium during the injection of Al₂O₃/SiO₂ CTAB foam. As indicated in Fig. 12a, the gas bubble can pass through the pore throat, depending on the gas bubble's viscoelasticity and the differences of the fluid pressures. In this situation, the gas bubble can deform and enter the pore throat since the fluid's driving force on the gas bubble is sufficiently high to dominate the supportive force of the pore throat's wall. After passing through the pore throat, the gas bubble will quickly regain its initial shape and size. The forces acting on the gas bubbles moving through the pore throats are shown in Fig. 12a. The oil droplet remained as residual oil is observed in Fig. 12a₅.

The same phenomenon has occurred in Fig. 12b where the foam bubble number 1 has caused the deformation of foam bubble number 2 when passing through the pore throat. The figure also shows gas bubble deformations when they are in contact with an oil droplet in the porous medium. As indicated, oil droplets are formed under these forces. With the deformation of the gas bubble due to its viscoelasticity, more forces are applied to the oil droplet and make an amount of it move toward production (Fig. 12: b₂ and b₃).

- New Form of Lamella Division

Lamella division is a well-known mechanism during foam injection [53]. In this mechanism, the foam bubble divides into two individual

ones when encountering a branch point with two or more pore throats [35]. In this research, this mechanism was found to be the predominant mechanism of bubble scale in the porous medium, however, with a distinctive new appearance. This new form of lamella division is called "bubble-bubble or bubble-induced lamella division" to differentiate it from the traditional form observed in the literature. The same form of this new lamella division was also observed by Yekeen et al. during the injection of SiO₂ and Al₂O₃ SDS foams [22]. In this mechanism, as shown in Fig. 13, instead of a branch point, other foam bubbles cause the lamella division.

- Formation and Development of Oil Threads in Porous Media

The deformation of gas bubbles occurs when they contact with the trapped oil droplets. With further contact, bubbles may recover to their spherical shape, which applies an elastic force on the oil droplet (Fig. 14). The elastic forces can change the droplet shape and mobilize it. As a result, once the trapped oil droplets are forced into the pores, the flowing gas bubbles can make them join the oil threads [7]. This observation mainly results from the viscoelasticity of the foam bubbles. Therefore, the residual oil is recovered by NPs-stabilized foam. In this situation, oil threads move in the pore throats (Fig. 14a) or on the pore walls (Fig. 14b). In both cases, they become thicker with a further foam injection.

- Neighbor-Wall Pinch-off Mechanism

This mechanism acts as a snap-off and lamella division, which are two important foam generation mechanisms in the porous media. As can be seen in Fig. 15, this kind of foam bubble division only happens when two bubbles try to flow simultaneously through the same pore throat. As the pore throat is narrow, it will not happen and, as a result, the second bubble flows into the first bubble and causes the first bubble to split into two parts [54,55]. Then, it can be regarded as lamella division.

- Snap-off

In this process, lamellae or bubbles are formed when gas-liquid surface is forced to go into

a narrow pore throat by the gas phase [56,57]. Fig. 16 shows the snap-off mechanism observed during the injection of Al₂O₃/SiO₂ CTAB foam.

- Foam Formation in the Porous Medium

Fig. 17 shows a typical microscopic image of the formation of foam bubbles in the porous media during the injection of $\text{Al}_2\text{O}_3/\text{SiO}_2$ CTAB foam. Foam generation in the porous media could be facilitated with

the presence of a surfactant and is beneficial to EOR. As indicated, with further injection, more and more foam bubbles are generated in the porous medium, which subsequently promotes the oil production

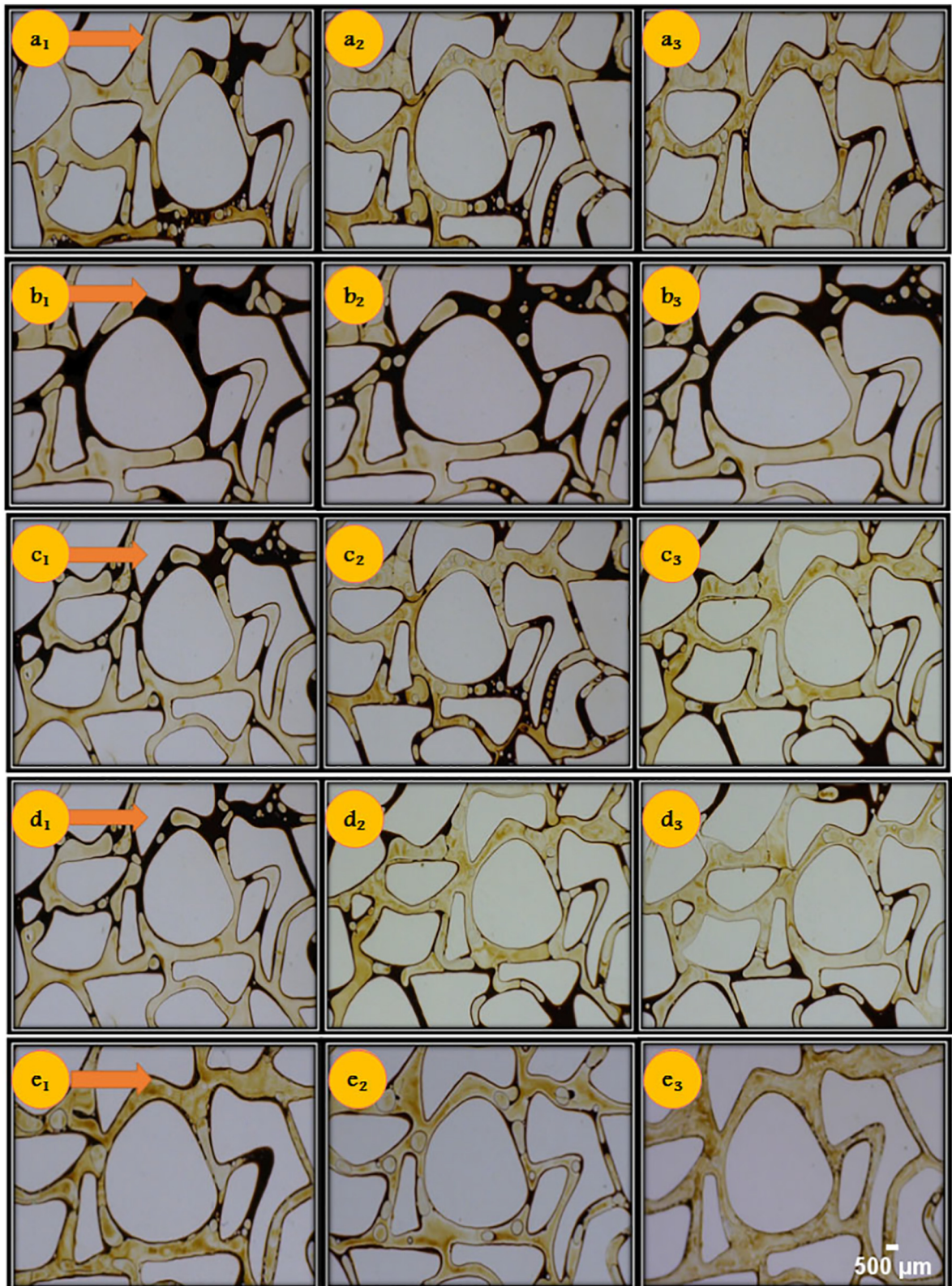


Fig. 10. Wettability alteration during injection of (a) DIW (b) N_2 gas (c) SiO_2 CTAB foam (d) Al_2O_3 CTAB foam (e) $\text{Al}_2\text{O}_3/\text{SiO}_2$ CTAB foam (The concentrations of NPs and CTAB were 0.04 wt% and 0.08 wt%, respectively). Subscripted numbers show the time passage.

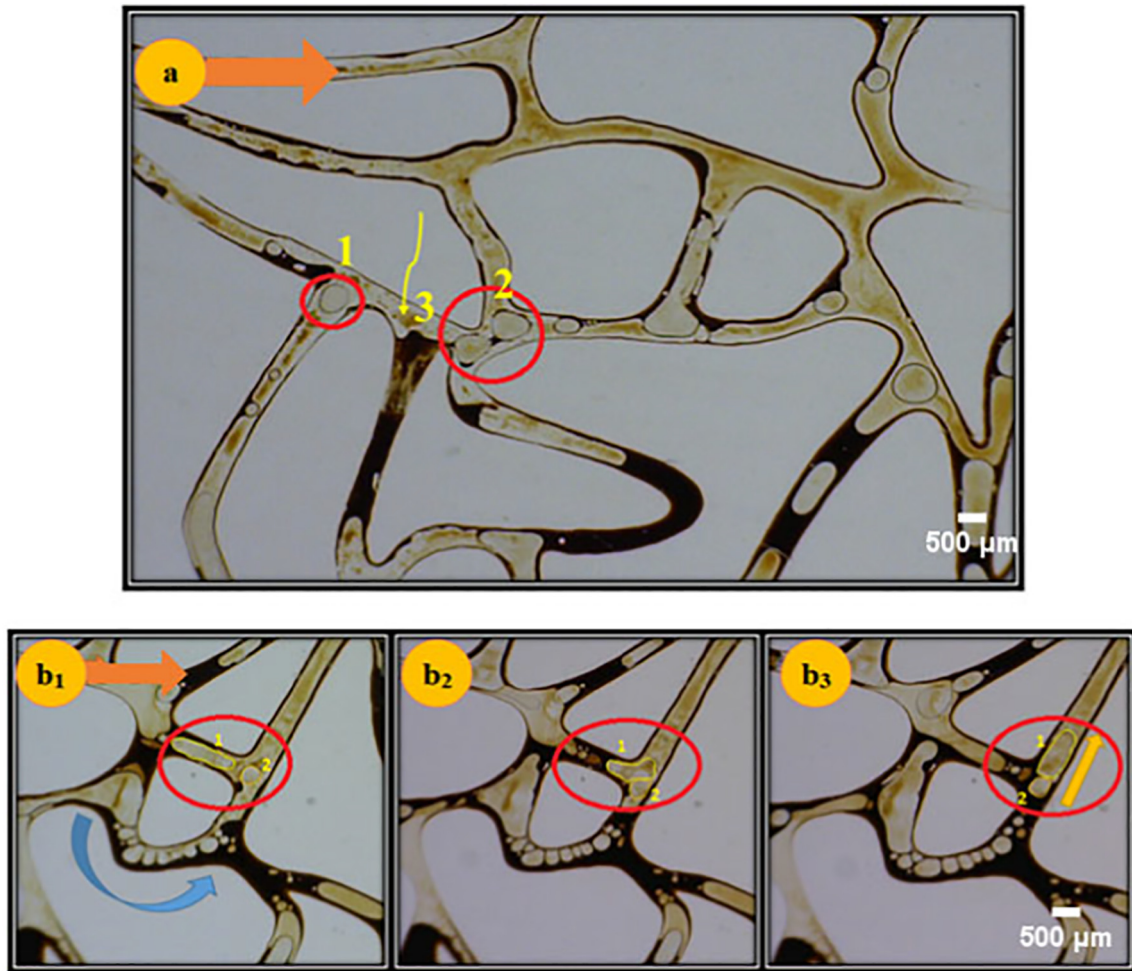


Fig. 11. Foam blockage mechanism during injection of $\text{Al}_2\text{O}_3/\text{SiO}_2$ CTAB foam in different zones of the porous medium (0.04 wt% $\text{Al}_2\text{O}_3/\text{SiO}_2$ NPs and 0.08 wt% CTAB). Subscripted numbers show the time passage.

mechanisms and leads to increased oil recovery. This confirms the efficiency of $\text{Al}_2\text{O}_3/\text{SiO}_2$ NPs in improving foam bubble stability in the porous media. In this regard, $\text{Al}_2\text{O}_3/\text{SiO}_2$ NPs take the role of improving the viscoelasticity of the foam lamellae and prevent bubbles from rupturing [58]. The intensity of foam generation was not this much in the presence of Al_2O_3 and SiO_2 NPs in CTAB foam. However, the same observation was found during the CTAB foam injection, but the foam bubbles were not stable.

- Driving Force of Gas Bubbles for Oil Displacement

Fig. 18 illustrates a new observation for oil droplet production in the porous medium during the injection of $\text{Al}_2\text{O}_3/\text{SiO}_2$ CTAB foam. As indicated, oil droplet has been separated into two parts with the driving force of the foam bubble, which comes from the emulsification effect of NPs and surfactant in the aqueous phase. Because gas bubbles prefer to remain spherical with the adsorption of CTAB onto the NPs at the water/ N_2 surface, the flowing gas bubbles accelerates the formation of emulsified oil droplets, as shown in Fig. 18.

3.6.3. Comparison of pressure drop/oil recovery of different fluids

Fig. 19 presents the oil recovery factor and the differential pressures (ΔP) of different injection scenarios. Overall, secondary (DIW) injection had no pressure drop fluctuation during injection into the porous

medium, simply beginning with an initial increase in differential pressure until the breakthrough at ~ 0.3 PV, decreasing with further injection, and leveling off at the end. On the contrary, in the tertiary mode, ΔP of injected fluids (except for N_2 gas injection) has seen an initial decrease, followed by a subsequent considerable increase. Differential pressure fluctuations are also observed with different foam injections. The highest and lowest ΔP belongs to $\text{Al}_2\text{O}_3/\text{SiO}_2$ CTAB foam and CTAB foam, respectively, which correspond to the highest and lowest oil recovery factors.

It is also clear to mention that pressure drops of $\text{Al}_2\text{O}_3/\text{SiO}_2$ CTAB foam have increased more rapidly as compared to those of others. This increase comes from the improved in-situ foam generation mechanisms in the porous medium with the addition of $\text{Al}_2\text{O}_3/\text{SiO}_2$ NPs to the aqueous phase of foam. The viscosity and the flow resistance of the $\text{Al}_2\text{O}_3/\text{SiO}_2$ CTAB foam in the system are much higher than those of water. This high viscosity can potentially plug the flow channels during water flooding which finally can lead to an increased swept area. Moreover, in the presence of a surfactant in the system, the nitrogen gas could form foam. As a result, the viscosity of the injected gas and the contact time of gas/oil increases. NPs are useful for stabilizing foam bubbles. They adsorb onto the foam lamellae and increase the film thickness and dilatational viscoelasticity. This indeed prevents the drainage of liquid and film thinning and enhances foam bubble stability. In this regard, the gas injection has the lowest pressure drop owing to the high permeability of porous media and low gas viscosity, which makes it easy to flow.

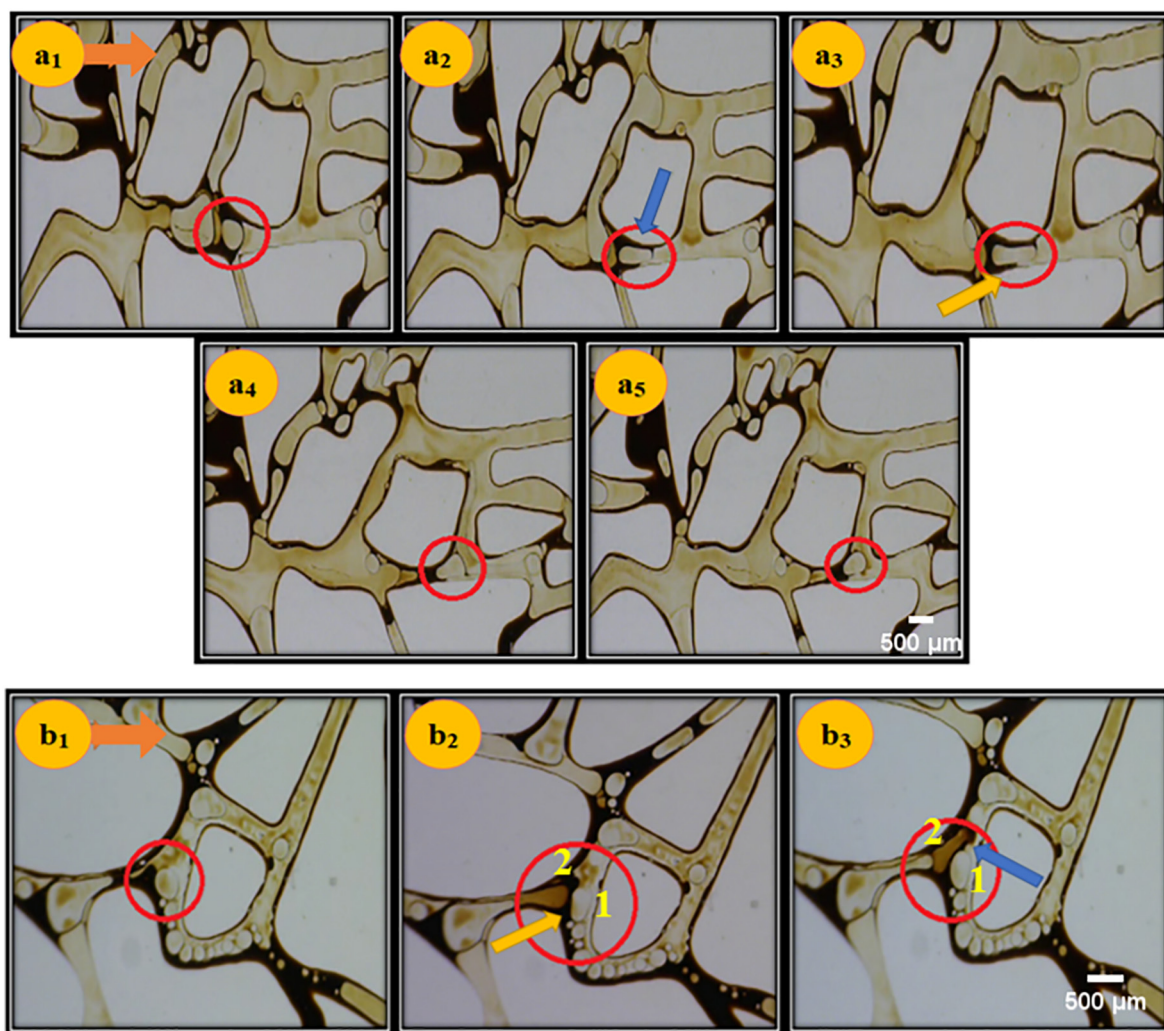


Fig. 12. Microscopic pictures of (a) gas bubble reshaping in a pore throat during $\text{Al}_2\text{O}_3/\text{SiO}_2$ -CTAB foam flooding. (b) Oil droplet formation under the action of gas bubbles. Subscripted numbers show the time passage.

Fig. 19b shows the oil recovery factors of different injected fluids. As indicated, the recovery factor of the water flooding stage is almost the same in all scenarios, standing at 18–19% OOIP. The oil recovery improves with foam injections (with or without NPs) due to the higher viscosity of foam that leads to enhanced sweep efficiency. Moreover, the oil/water IFT is reduced by the presence of the surfactant in the foam which ultimately increases the efficiency of oil displacement. It was also revealed that the ultimate oil recovery factors of foam flooding are in the range of 51–92% OOIP, which is much higher than that of conventional gas flooding (i.e. 23% OOIP). In this regard, the highest ultimate oil recovery is observed with $\text{Al}_2\text{O}_3/\text{SiO}_2$ CTAB foam at 92% OOIP. Comparing the macroscopic images with these results, it is obvious to mention that the area affected by foam injection in dual porous media (see Fig. 9) is considerably larger than that by other conventional water and gas flooding since foam can spread to the other parts of the heterogeneous media, as discussed before.

4. Conclusions

In this research, we attempted to compare the effects of three NPs including Al_2O_3 , SiO_2 , and $\text{Al}_2\text{O}_3/\text{SiO}_2$ for EOR. The following findings were resulted through different static and dynamic analyses:

- The order of foam stability improvement in the presence of NPs and a crude oil sample was obtained as follows:

$\text{Al}_2\text{O}_3/\text{SiO}_2$ CTAB foam > Al_2O_3 CTAB foam > SiO_2 CTAB foam

This confirms the efficiency of the synthesized $\text{Al}_2\text{O}_3/\text{SiO}_2$ for EOR.

- The addition of NPs (i.e. Al_2O_3 , SiO_2 , and $\text{Al}_2\text{O}_3/\text{SiO}_2$) to the foam solutions presented a great wettability alteration toward a water-wet condition both at static and dynamic experiments via synergistic effects of NPs and CTAB.
- The addition of $\text{Al}_2\text{O}_3/\text{SiO}_2$ NPs to CTAB foam increased the bubble foam deformability and viscoelasticity both at the static and dynamic conditions. In the porous medium, it was observed that it can significantly improve the foam diversion to the unswept areas and thus produce more oil. Stable viscoelastic foam bubbles can also continuously generate new foam bubbles in the porous medium when contacting each other, which led to the observation of a new form of lamella division called “bubble-Bubble lamella Division”. To the best knowledge of our knowledge, this mechanism has not been yet observed in the previous studies.
- $\text{Al}_2\text{O}_3/\text{SiO}_2$ CTAB foam injection resulted in the most macroscopic sweep efficiency and microscopic displacement efficiency at lower injected PV, which is more economical as compared to other NPs.

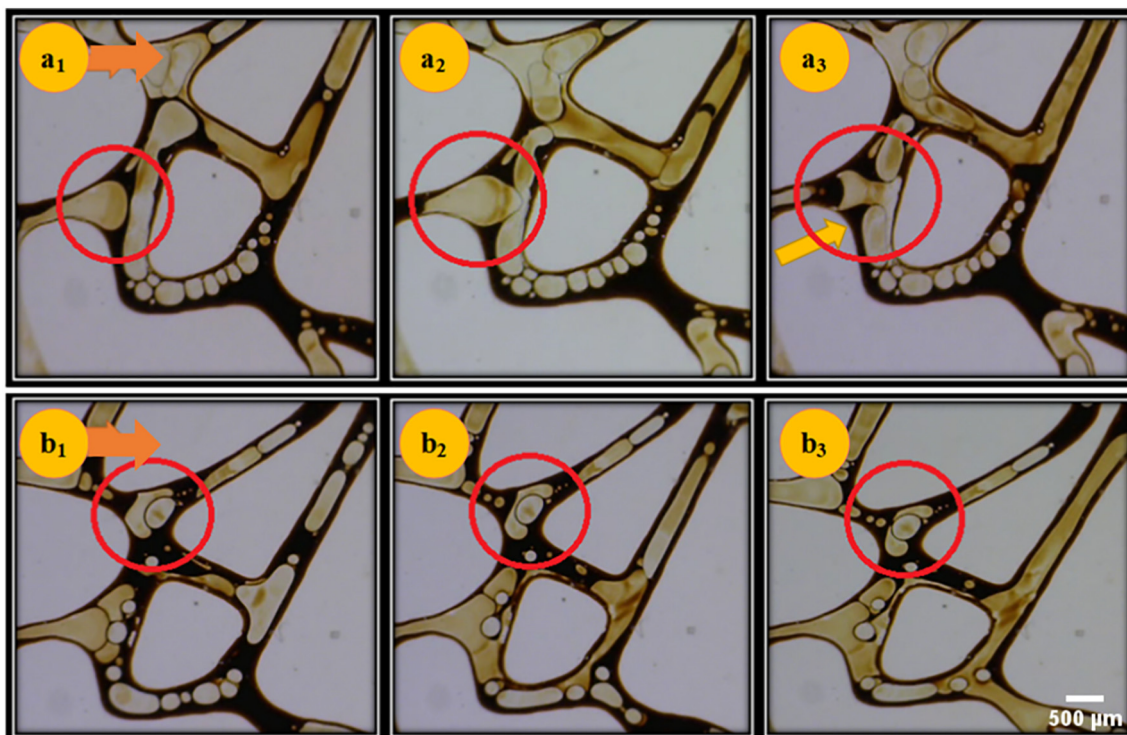


Fig. 13. A new form of Lamella division, called “bubble-bubble or bubble-induced lamella division”, observed in the porous medium during injection of $\text{Al}_2\text{O}_3/\text{SiO}_2$ CTAB foam (0.04 wt% $\text{Al}_2\text{O}_3/\text{SiO}_2$ NPs and 0.08 wt% CTAB). Subscripted numbers show the time passage.

- Ultimate oil recoveries confirmed that adding NPs to the foam solution can enhance foam performance. In this regard, $\text{Al}_2\text{O}_3/\text{SiO}_2$ CTAB foam presented the highest oil recovery factor.
- The main objective of the current work was to question the simultaneous application of efficient NPs for EOR investigated in previous studies as a nanocomposite form to make the most of the synergy.

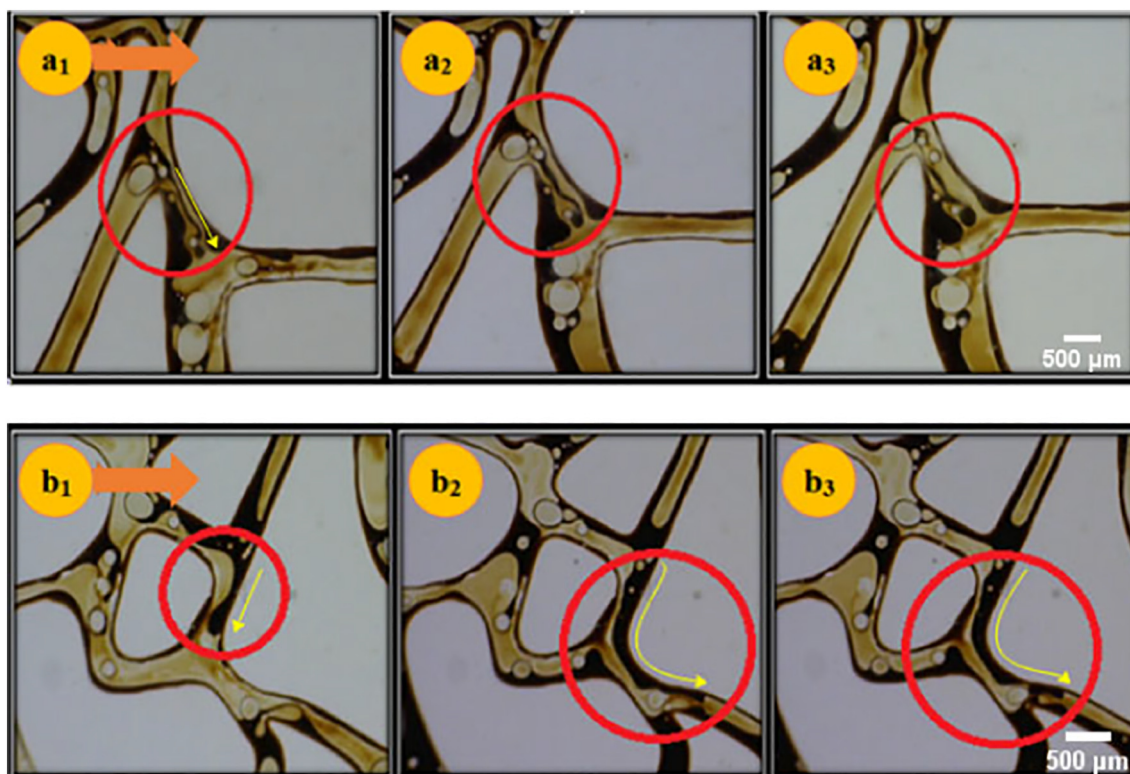


Fig. 14. Pore-level images of formation and transportation of oil threads in the porous medium during injection of $\text{Al}_2\text{O}_3/\text{SiO}_2$ CTAB foam in various parts of the model (0.04 wt% $\text{Al}_2\text{O}_3/\text{SiO}_2$ NPs and 0.08 wt% CTAB). Subscripted numbers show the time passage.

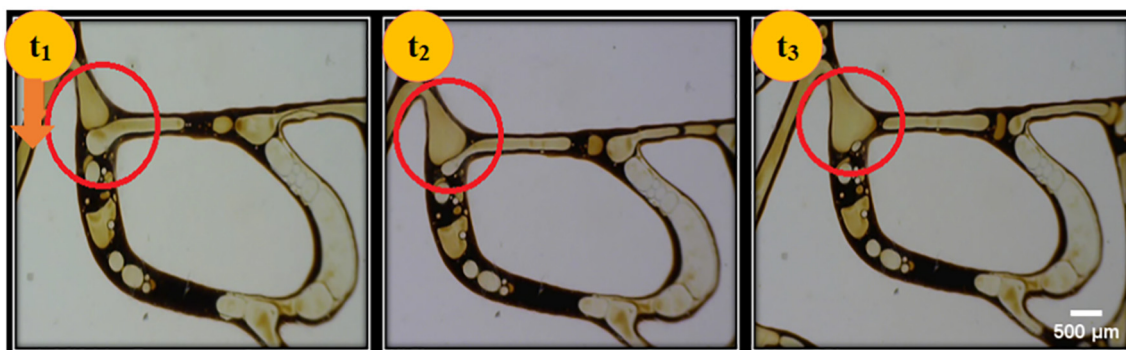


Fig. 15. Neighbor-wall pinch off observed in the porous medium during injection of $\text{Al}_2\text{O}_3/\text{SiO}_2$ CTAB foam in various parts of the model (0.04 wt% $\text{Al}_2\text{O}_3/\text{SiO}_2$ NPs and 0.08 wt% CTAB). Subscripted numbers show the time passage.

The current promising results are a part of our initial investigation on this area and yet require further investigations.

CRediT authorship contribution statement

Hosein Rezvani:Data curation, Writing - original draft, Investigation, Writing - review & editing.**Donya Panahpoori:**Data curation, Writing - original draft, Investigation.**Masoud Riazi:**Supervision, Conceptualization, Project administration, Writing - review & editing.**Rafat Parsaei:**Supervision, Methodology.**Morteza Tabaei:**Supervision.**Farid B. Cortés:**Methodology, Writing - review & editing.

Declaration of competing interest

The authors declare that they have no known competing financial interests or personal relationships that could have appeared to influence the work reported in this paper.

Acknowledgments

We would like to thank National Iranian Oil Company (NIOC) for funding this project and providing us the crude oil sample and related information.



Fig. 16. Snap-off mechanism observed in the porous medium during the injection of $\text{Al}_2\text{O}_3/\text{SiO}_2$ CTAB foam (0.04 wt% $\text{Al}_2\text{O}_3/\text{SiO}_2$ NPs and 0.08 wt% CTAB). Subscripted numbers show the time passage.

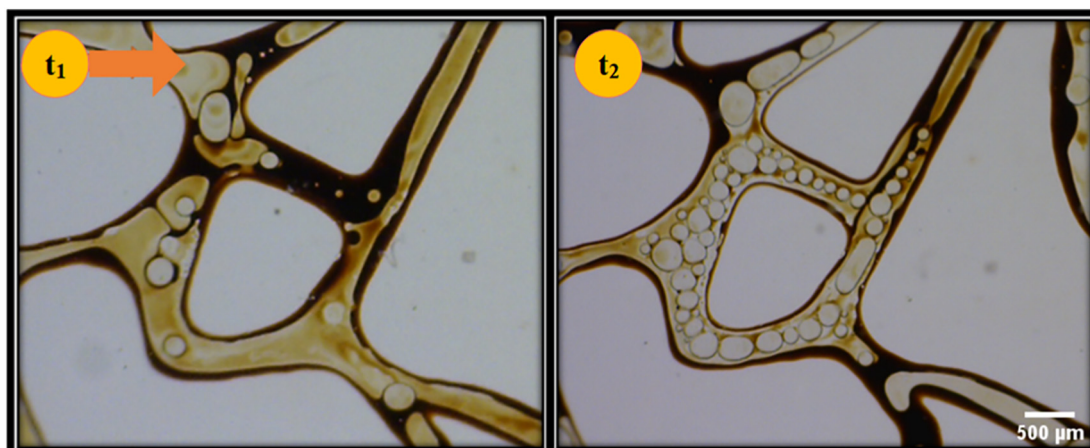


Fig. 17. Pore-level images of foam bubble formation in the porous medium during injection of $\text{Al}_2\text{O}_3/\text{SiO}_2$ CTAB foam (0.04 wt% $\text{Al}_2\text{O}_3/\text{SiO}_2$ NPs and 0.08 wt% CTAB). Subscripted numbers show the time passage.

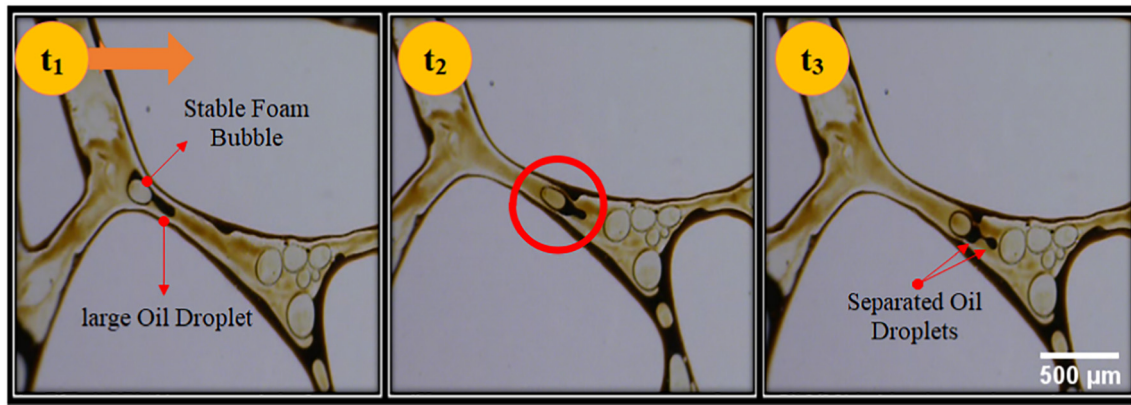


Fig. 18. Microscopic image of an oil droplet driven by a foam bubble. The phenomenon is the residual oil mobilization by foam flooding in an oil-wet porous media in which micro-elastic forces of gas bubbles mobilize the oil droplets. Subscripted numbers show the time passage.

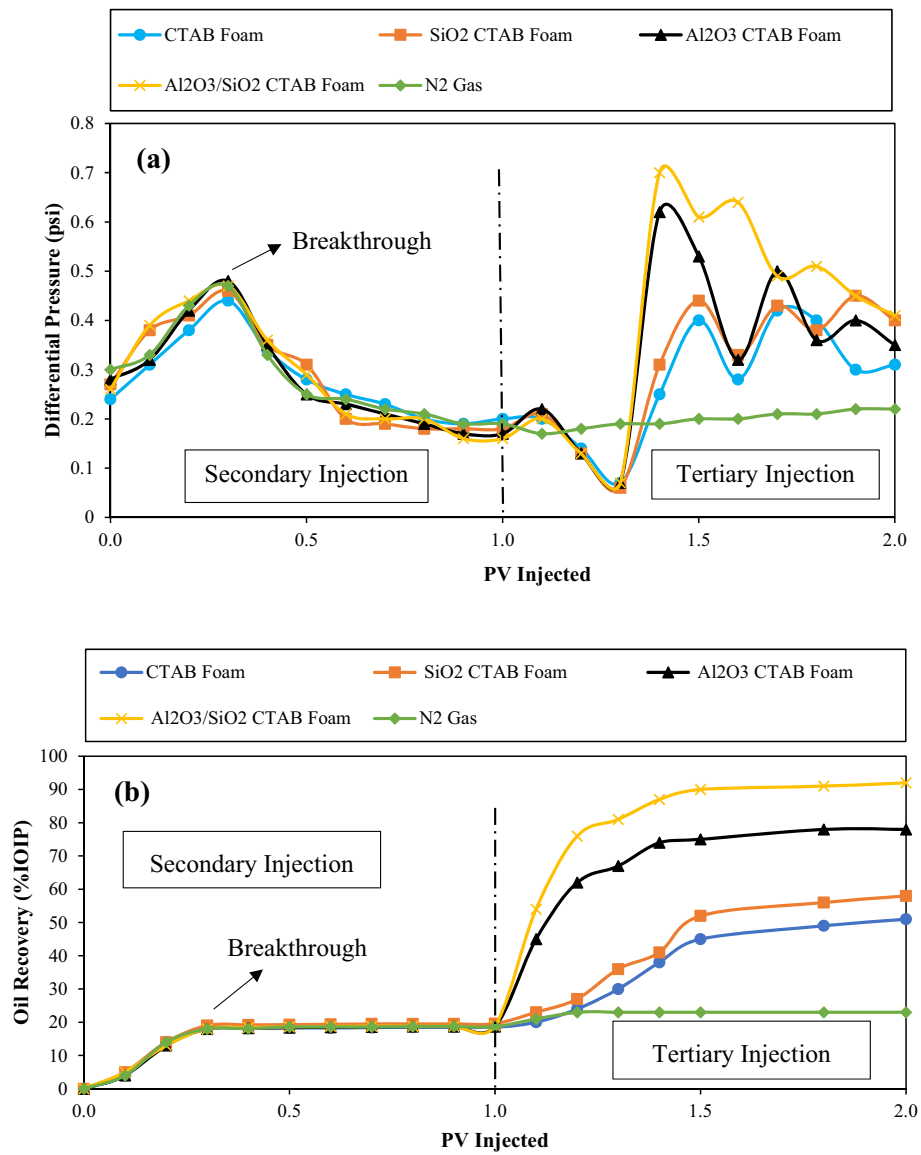


Fig. 19. (a) Differential pressure (b) oil recovery factor of different injected fluids.

References

- [1] A. Rahim Risal, M.A. Manan, N. Yekeen, A. Mohamed Samin, N.B. Azli, J. Dispers. Sci. Technol. 39 (2018) 1767.
- [2] D. Kong, Y. Li, M. Yu, R. Ma, H. Guo, Y. Peng, S. Xu, H. Yan, Colloids Surf. A Physicochem. Eng. Asp. 570 (2019) 22.
- [3] Y. Hurtado, C. Beltrán, R.D. Zabala, S.H. Lopera, C.A. Franco, N.N. Nassar, F.B. Cortés, Energy Fuel 32 (2018) 5824.
- [4] A. Aroonsri, A.J. Worthen, T. Hariz, K.P. Johnston, C. Huh, S.L. Bryant, SPE Annual Technical Conference and Exhibition, Society of Petroleum Engineers, 2013.
- [5] V. Kumar, N. Pal, A.K. Jangir, D.L. Manyala, D. Varade, A. Mandal, K. Kuperkar, Colloids Surf. A Physicochem. Eng. Asp. 588 (2020), 124362.
- [6] D. Panahpoori, B. Dehdari, M. Riazi, R. Parsaei, Saint Petersburg 2018, 2018.
- [7] T. Lu, Z. Li, Y. Zhou, Energies 10 (2017) 560.
- [8] W. Yang, T. Wang, Z. Fan, Energy Fuel 31 (2017) 9016.
- [9] D. Mo, J. Yu, N. Liu, R.L. Lee, SPE Annual Technical Conference and Exhibition, Society of Petroleum Engineers, 2012.
- [10] S. Kumar, A. Mandal, Appl. Surf. Sci. 420 (2017) 9.
- [11] S. Alzobaidi, M. Lotfollahi, I. Kim, K.P. Johnston, D.A. DiCarlo, Energy Fuel 31 (2017), 10680.
- [12] A.J. Worthen, H.G. Bagaria, Y. Chen, S.L. Bryant, C. Huh, K.P. Johnston, J. Colloid Interface Sci. 391 (2013) 142.
- [13] A. Khalilnezhad, H. Rezvani, P. Ganji, Y. Kazemzadeh, Oil & Gas Science and Technology-Revue d'IFP Energies Nouvelles 74 (2019) 39.
- [14] N. Yekeen, M.A. Manan, A.K. Idris, E. Padmanabhan, R. Junin, A.M. Samin, A.O. Gbadamosi, I. Oguamah, J. Pet. Sci. Eng. 164 (2018) 43.
- [15] S. Kumar, P. Panigrahi, R.K. Saw, A. Mandal, Energy Fuel 30 (2016) 2846.
- [16] Y. Hurtado, S. Avila, F.B. Cortés, C.A. Franco Ariza, M. Riazi, V.I.I. Escuela De Verano, New Technologies in Productivity and Enhanced Recovery of Oil and Gas, Hotel Dann Carlton-Berlfort, Medellin, Columbia, 2019 (2019).
- [17] C. Qian, A. Telmadarreie, M. Dong, S. Bryant, SPE Western Regional Meeting, Society of Petroleum Engineers, 2019.
- [18] D. Panahpoori, H. Rezvani, R. Parsaei, M. Riazi, J. Pet. Sci. Eng. 183 (2019), 106411.
- [19] S. Betancur, F. Carrasco-Marín, C.A. Franco, F.B. Cortés, Ind. Eng. Chem. Res. 57 (2018), 12367.
- [20] M. Manan, S. Farad, A. Piroozian, M. Esmail, Pet. Sci. Technol. 33 (2015) 1286.
- [21] A.E. Bayat, K. Rajaei, R. Junin, Colloids Surf. A Physicochem. Eng. Asp. 511 (2016) 222.
- [22] N. Yekeen, M.A. Manan, A.K. Idris, A.M. Samin, A.R. Risal, J. Pet. Sci. Eng. 159 (2017) 115.
- [23] A. Rognmo, S. Heldal, M. Fernø, Fuel 216 (2018) 621.
- [24] A.R. Risal, M.A. Manan, N. Yekeen, N.B. Azli, A.M. Samin, X.K. Tan, Pet. Sci. 16 (2019) 344.
- [25] M.I. Mobarakeh, A. Saffar-Teluri, S.H. Tabrizi, Res. Chem. Intermed. 41 (2015) 6625.
- [26] X. Duan, D. Yuan, D. Pan, C. Luan, H. Sun, D. Xu, M. Lv, J. Mater. Sci. 40 (2005) 2975.
- [27] H. Rezvani, A. Khalilnezhad, A.A. Sadeghi-Bagherabadi, 80th EAGE Conference and Exhibition 2018, 2018.
- [28] H. Rezvani, A. Khalilnezhad, P. Ganji, Y. Kazemzadeh, J. Mol. Liq. 252 (2018) 158.
- [29] H. Rezvani, M. Tabaei, M. Riazi, Materials Research Express 6 (2019), 085505.
- [30] J. Ayers, J. Cryst. Growth 135 (1994) 71.
- [31] S. Zhang, Q. Lan, Q. Liu, J. Xu, D. Sun, Colloids Surf. A Physicochem. Eng. Asp. 317 (2008) 406.
- [32] B.P. Binks, J.A. Rodrigues, W.J. Frith, Langmuir 23 (2007) 3626.
- [33] Z. Bi, W. Liao, L. Qi, Appl. Surf. Sci. 221 (2004) 25.
- [34] R. Songolzadeh, J. Moghadasi, Colloid Polym. Sci. 295 (2017) 145.
- [35] T. Fu, Y. Ma, D. Funfschilling, H.Z. Li, Chem. Eng. Sci. 66 (2011) 4184.
- [36] I. Garcia-Mateos, M. Mercedes Velazquez, L.J. Rodriguez, Langmuir 6 (1990) 1078.
- [37] S. Li, C. Qiao, Z. Li, S. Wanambwa, Energy Fuel 31 (2017) 1478.
- [38] A.C.Y. Tiong, I.S. Tan, H.C.Y. Foo, IOP Conference Series: Materials Science and Engineering, IOP Publishing, 2019 012058.
- [39] R. Farajzadeh, A. Andrianov, R. Krastev, G. Hirasaki, W.R. Rossen, Adv. Colloid Interf. Sci. 183 (2012) 1.
- [40] S.J.D. Sofla, L.A. James, Y. Zhang, E3S Web of Conferences, EDP Sciences, 2019, p. 03004.
- [41] N.K. Jha, M. Lebedev, S. Iglauer, M. Ali, H. Roshan, A. Barifcani, J.S. Sangwai, M. Sarmadivaleh, J. Colloid Interface Sci. 562 (2020) 370.
- [42] D.T. Wasan, A.D. Nikolov, Nature 423 (2003) 156.
- [43] M. Franco-Aguirre, R.D. Zabala, S.H. Lopera, C.A. Franco, F.B. Cortés, J. Nat. Gas Sci. Eng. 51 (2018) 53.
- [44] H. Zhang, A. Nikolov, D. Wasan, Energy Fuel 28 (2014) 3002.
- [45] D. Wasan, A. Nikolov, K. Kondiparty, Curr. Opin. Colloid Interface Sci. 16 (2011) 344.
- [46] D. Langevin, Adv. Colloid Interf. Sci. 88 (2000) 209.
- [47] P. Koelsch, H. Motschmann, Langmuir 21 (2005) 6265.
- [48] N. Pal, N. Kumar, A. Mandal, Langmuir 35 (2019) 2655.
- [49] M.J. Rosen, J.T. Kunjappu, Surfactants and Interfacial Phenomena, John Wiley & Sons, 2012.
- [50] Q. Sun, Z. Li, S. Li, L. Jiang, J. Wang, P. Wang, Energy Fuel 28 (2014) 2384.
- [51] Y. Murai, T. Shiratori, I. Kumagai, P.A. Rühls, P. Fischer, Flow Meas. Instrum. 41 (2015) 121.
- [52] M. Almahfood, B. Bai, J. Pet. Sci. Eng. 171 (2018) 196.
- [53] B. Géraud, Y. Méheust, I. Cantat, B. Dollet, Phys. Rev. Lett. 118 (2017), 098003.
- [54] D. Vecchiolla, V. Giri, S.L. Biswal, Soft Matter 14 (2018) 9312.
- [55] R. Lontas, K. Ma, G.J. Hirasaki, S.L. Biswal, Soft Matter 9 (2013), 10971.
- [56] A. Falls, G. Hirasaki, T. Patzek, D. Gauglitz, D. Miller, T. Ratulowski, SPE Reserv. Eng. 3 (1988) 884.
- [57] W.R. Rossen, Colloids Surf. A Physicochem. Eng. Asp. 166 (2000) 101.
- [58] D.Y. Zang, E. Rio, D. Langevin, B. Wei, B.P. Binks, Eur. Phys. J. E Soft Matter 31 (2010) 125.